

1 Differential requirement of NPHP1 for compartmentalized protein localization during

2 photoreceptor outer segment development and maintenance

3

4 Poppy Datta^{a,b,#}, J. Thomas Cribbs^{a,b,#}, and Seongjin Seo^{a,b,*}

5

⁶ Department of Ophthalmology and Visual Sciences, The University of Iowa Carver College of Medicine, Iowa
⁷ City, IA 52242, U.S.A.

⁸ ^bInstitute for Vision Research, The University of Iowa, Iowa City, IA 52242, U.S.A.

9

10

11 #Equally contributed

12 *To whom correspondence should be addressed:

13 Seongjin Seo, PhD

14 Department of Ophthalmology and Visual Sciences

15 University of Iowa College of Medicine

16 375 Newton Rd

17 3181D MERF

18 Iowa City, IA 52242, U.S.

19 Phone: 1-319-353-4477

20 Email: seongjin-seo@uiowa.edu

21

22 **Running title: Roles of NPHP1 in photoreceptors**

23 **Keywords:** cilia; ciliary gate; compartmentalization; inherited retinal degeneration; nonsense-associated altered
24 splicing; protein confinement; transition zone

25 Abstract

26 Nephrocystin (NPHP1) is a ciliary transition zone protein and its ablation causes nephronophthisis (NPHP) with
27 partially penetrant retinal dystrophy. However, the precise requirements of NPHP1 in photoreceptors are not well
28 understood. Here, we characterize retinal degeneration in a mouse model of NPHP1 and show that NPHP1 is
29 required to prevent infiltration of inner segment plasma membrane proteins into the outer segment during the
30 photoreceptor maturation. We demonstrate that *Nphp1* gene-trap mutant mice, which were previously described
31 as null, are in fact hypomorphs due to the production of a small quantity of functional mRNAs derived from
32 nonsense-associated altered splicing and skipping of two exons including the one harboring the gene-trap. In
33 homozygous mutant animals, inner segment plasma membrane proteins such as syntaxin-3 (STX3),
34 synaptosomal-associated protein 25 (SNAP25), and interphotoreceptor matrix proteoglycan 2 (IMPG2)
35 accumulate in the outer segment when outer segments are actively elongating. This phenotype, however, is
36 spontaneously ameliorated after the outer segment elongation is completed. Retinal degeneration also occurs
37 temporarily during the photoreceptor maturation but stops afterward. We further show that *Nphp1* genetically
38 interacts with *Cep290*, another NPHP gene, and that a reduction of *Cep290* gene dose results in retinal
39 degeneration that continues until adulthood in *Nphp1* mutant mice. These findings demonstrate that NPHP1 is
40 required for the confinement of inner segment plasma membrane proteins during the outer segment development,
41 but its requirement diminishes as photoreceptors mature. Our study also suggests that additional mutations in other
42 NPHP genes may influence the penetrance of retinopathy in human NPHP1 patients.

43

44 Introduction

45 Photoreceptor cells in the retina are structurally and functionally compartmentalized. Proteins that transduce light
46 into chemical and electrical signals are confined to an apical compartment called the outer segment (OS). This
47 structure is an elaborate modification of primary cilia, which exist in most cells in vertebrates (see [1, 2] for a
48 comprehensive review). In contrast, energy production and protein/lipid synthesis occur in another compartment,
49 the inner segment (IS). Constituents of the OS are synthesized in the IS and transported to the OS through a narrow
50 channel, the connecting cilium. The connecting cilium is equivalent to the transition zone in primary cilia and
51 plays critical roles in regulating protein trafficking and confinement between the IS and the OS [3].

52

53 Nephrocystin (also known as NPHP1) is a protein that localizes to the connecting cilium in photoreceptors and
54 the transition zone in primary cilia [4-9]. At the transition zone, NPHP1 is a part of a multi-protein complex that
55 functions as a gate to control protein trafficking in and out of the ciliary compartment [8-13]. Ablation of
56 individual components in this complex causes a group of related diseases, including nephronophthisis (NPHP),
57 Joubert syndrome (JBTS), and Meckel-Gruber syndrome (MKS) [14, 15]. Retinal anomalies are common in
58 patients with these diseases. While *NPHP1* is primarily associated with NPHP [16-19], a subset (6-10%) of
59 NPHP1 patients exhibits retinal dystrophy as an extra-renal manifestation [19, 20]. This suggests a role of NPHP1
60 in photoreceptors. However, its precise functions in photoreceptors and the molecular/genetic basis of the
61 incomplete penetrance are not well understood.

62

63 Two NPHP1 mouse models have been described thus far. In one model (*Nphp1^{del20}*), the last exon (exon 20) was
64 deleted, and homozygous mutant animals displayed severe retinal degeneration with OS morphogenesis defects
65 [5, 21]. *Nphp1^{del20/del20}* animals also exhibited male infertility due to a defect in spermatogenesis [21]. The second
66 model (*Nphp1^{neo}*; hereafter referred to as *Nphp1^{gt}*) was generated by an insertion of a gene-trap (a *PGK-neo-pA*
67 cassette) into exon 4 (**S1 Fig**) [22]. This mutation is expected to generate a null allele because it disrupts the
68 reading frame of *Nphp1*. However, retinal degeneration in this model is significantly milder than that of *Nphp1^{del20}*
69 mice: a slight reduction of the photoreceptor cell layer was observed at postnatal (P) day P21 and 2 months of age,

70 and rhodopsin (RHO) trafficking was only marginally affected. Retinal phenotypes in older animals were not
71 reported. The basis of this phenotypic difference in severity between these two mouse models is unknown, but
72 disparities in the genetic background were suggested as a potential contributing factor [22]. Currently, only the
73 *Nphp1^{gt}* model is available to the research community and has been used in several studies to investigate genetic
74 interactions with other ciliopathy genes [9, 23, 24].

75

76 We previously proposed that the OS acts as a sink for membrane proteins because of its large size, high membrane
77 content, and continuous renewal [3]. This also suggests that accumulation of IS membrane proteins in the OS
78 would be a common pathomechanism of retinal degenerations associated with ciliary gate defects. Indeed, IS
79 plasma membrane-associated proteins including syntaxin-3 (STX3), syntaxin-binding protein 1 (STXBP1),
80 synaptosomal-associated protein 25 (SNAP25), and interphotoreceptor matrix proteoglycan 2 (IMPG2) rapidly
81 accumulate in the OS when the function of CEP290, another component of the ciliary gate complex, is
82 compromised [25]. Notably, inactivating mutations in *CEP290* cause Leber congenital amaurosis (LCA), an early-
83 onset severe retinal degeneration, in humans [26-29]. In this work, we sought to determine the requirement of
84 NPHP1 for protein confinement in photoreceptors and test whether the aforementioned pathomechanism underlies
85 retinal degeneration in *NPHP1*-associated retinopathies.

86

87 Materials and methods

88 Mouse and genotyping

89 *Nphp1^{gt}* and *Cep290^{fl}* mice were previously described [22, 30] and obtained from the Jackson laboratory
90 (*Nphp1^{tm1Jgg}*/J, #013169; *Cep290^{tm1Jgg}*/J, #013701). *iCre75* mice were a generous gift from Dr. Ching-Kang Chen
91 [31]. The lack of *rd1* mutation (in *Pde6b*) was confirmed by PCR using primers described in [25]. The *rd8*
92 mutation (in *Crbl*) was eliminated by breeding. All animals used in this study were *Pde6b*^{+/+}; *Crbl*^{+/+}. For
93 genotyping, mouse tail snips were collected at the time of weaning (P19-P24) or after euthanasia. Tail DNAs were
94 extracted by Proteinase K digestion (Sigma-Aldrich; RPROTK-RO) in Tail Lysis Buffer (10 mM Tris pH 8.0, 100
95 mM NaCl, 10 mM EDTA, 1% SDS, 0.3 mg/ml Proteinase K) followed by ethanol precipitation. Genotyping was
96 conducted by PCR using GoTaq G2 Flexi DNA polymerase (Promega) and primers listed in **Table 1**. PCR
97 protocols are available upon request. All animals were maintained in 12-hour light/dark cycles and fed *ad libitum*
98 standard mouse chow. All animal procedures were approved by the Institutional Animal Care and Use Committee
99 (IACUC) of the University of Iowa (Protocol#: 8011301) and conducted following the recommendations in the
100 Guide for the Care and Use of Laboratory Animals of the National Institutes of Health.

101

102 Table 1. Primers used in this study.

Purpose	Primer	Sequence	PCR product
<i>Nphp1</i> RT-PCR	F1-mNPHP1-RT	GTGCTCTGGAACCGAGTAAA	wt: 991 bp gt: 805 bp
	R1-mNPHP1-RT	TGTCTGCTGAGAACCTGTATG	
<i>Nphp1</i> genotyping	F-mNPHP1-WT	ACATTATGGAATCTGGGGTAG	wt: 289 bp gt: ~400 bp
	R-mNPHP1-comm	CCCCGCTAGAGTATGGTCTG	
	F-mNPHP1-GT	CGCCTTCTATCGCCTTCTTG	
<i>iCre75</i>	F-iCre75	TCAGTGCCTGGAGTTGCGCTGTGG	wt: none Tg: 650 bp
	R-iCre75	CTTAAAGGCCAGGGCCTGCTTGGC	
<i>Cep290^{fl}</i> genotyping	R2-Cep290-wt	GAATGCCGCTACAGAAGAA	wt: 535 bp fl: 426 bp
	F2-Cep290-comm	CAGCAGCTGAGGAACGTATAA	
	R2-Cep290-mut	CTACCGGTGGATGTGGAATG	
<i>Crbl</i> / <i>rd8</i> genotyping	F3-mCrb1-wt	GAAGACAGCTACAGTTCTCTC	wt: 388 bp rd8: 388 bp (separate reactions)
	R3-mCrb1-comm	CACCTATGGACGGACATTTA	
	F3-mCrb1-rd8	GAAGACAGCTACAGTTCTCTG	

103

104

105 **Plasmids and antibodies**

106 A full-length mouse *Nphp1* coding sequence (BC118953) was obtained from Transomic Technologies. FLAG-
107 tagged NPHP1 expression vectors (pCS2FLAG-NPHP1 (full-length), pCS2FLAG-NPHP1 Δ(49-110), and
108 pCS2FLAG-NPHP1 aa242-685) were generated by inserting PCR-amplified DNA fragments into the EcoRI-Xhol
109 sites of the pCS2FLAG plasmid, which was produced by replacing the 6x Myc tag with a 3x FLAG tag in the
110 pCS2+MT vector [32], using a GenBuilder cloning kit (GenScript). pCS2HA-NPHP1 and pCS2HA-NPHP1 Δ(49-
111 110) were generated by inserting the same PCR fragments into the pCS2HA vector [25]. Expression vectors
112 pEGFP-NPHP2 and pEGFP-NPHP5 were generous gifts from Drs. Val C. Sheffield and William Y. Tsang,
113 respectively. All constructs were sequence-verified by Sanger sequencing. Antibodies used for immunoblotting
114 and immunohistochemistry are described in **Table 2**.

115

116 **Table 2. Antibodies used in this study.**

Antibody	Source	Cat#	Verification
mouse anti-β-actin monoclonal (clone: AC-15)	Sigma-Aldrich	A1978	[33], [34]
mouse anti-ABCA4 monoclonal (clone: 3F4)	EMD Millipore	MABN2439	[35, 36]
Rabbit anti-ARL13B polyclonal	ProteinTech	17711-1-AP	[37]
mouse anti-FLAG monoclonal (clone: M2)	Sigma-Aldrich	F1804	not applicable
rabbit anti-GFP monoclonal	Invitrogen	G10362	not applicable
rabbit anti-GNAT2 polyclonal	Abcam	ab97501	[38]
rat anti-HA monoclonal (clone: 3F10)	Sigma/Roche	12158167001	not applicable
rabbit anti-IMPG2 polyclonal	Sigma-Aldrich	HPA008779	[25, 39]
rabbit anti-NPHP1 polyclonal (for immunoblotting)	Abclonal	A6674	this study
rabbit anti-NPHP1 polyclonal (for immunohistochemistry)	Invitrogen	PA1-25150	this study
rabbit anti-OPN1MW polyclonal	EMD Millipore	AB5405	[40, 41]
rabbit anti-PDE6B polyclonal	ProteinTech	22063-1-AP	[38]
mouse anti-polyglutamylation monoclonal (clone: GT335)	AdipoGen	AG-20B-0020-C100	[42, 43]
rabbit anti-PRPH2 polyclonal	ProteinTech	18109-1-AP	[38]
mouse anti-RHO monoclonal (clone: 1D4)	EMD Millipore	MAB5356	[44]
rabbit anti-ROM1 polyclonal	ProteinTech	21984-1-AP	[38]
rabbit anti-RPGRIP1L polyclonal	ProteinTech	55160-1-AP	this study; S2 Fig

mouse anti-SNAP25 monoclonal (clone: SMI81)	Abcam	ab24737	[38]
mouse anti-STX3 monoclonal (clone: 1-146)	EMD Millipore	MAB2258	[34]
rabbit anti-STXBP1 polyclonal	ProteinTech	11459-1-AP	[38]

117

118

119 **Immunoblotting**

120 To extract proteins from mouse testes, animals were euthanized by CO₂ asphyxiation followed by cervical
121 dislocation, and testicles were removed. Collected testicles were homogenized with Polytron PT 1200E
122 (Kinematica) in an ice-cold lysis buffer (50 mM HEPES pH7.0, 150 mM NaCl, 2 mM MgCl₂, 2 mM EGTA, 1%
123 Triton X-100) supplemented with Protease Inhibitor Cocktail (Bimake). Homogenates were clarified by
124 centrifugation at 20,000x g for 15 min at 4 °C and supernatants were collected. Protein concentrations were
125 measured using a DC Protein Assay kit (Bio-Rad) with BSA protein standards and AccuSkan GO
126 spectrophotometer (Fisher Scientific). Fifty µg of proteins were mixed with NuPAGE LDS Sample Buffer
127 (Invitrogen) and Reducing Agent (Invitrogen) and loaded on a 4-12% (wt/vol) NuPAGE Bis-Tris gel (Invitrogen).
128 After electrophoresis, proteins were transferred to a 0.45-µm nitrocellulose membrane (Bio-Rad). Immunoblotting
129 was performed following standard protocols, and primary antibodies used are listed in **Table 2**. Proteins were
130 detected with horseradish peroxidase (HRP)-linked anti-mouse IgG and anti-rabbit IgG secondary antibodies (Cell
131 Signaling) and SuperSignal West Dura Extended Duration Substrate (Thermo Scientific). Images were taken with
132 a ChemiDoc system (Bio-Rad).

133

134 **Immunohistochemistry**

135 Mouse eyes were collected, fixed, and embedded in Neg-50 Frozen Section Medium (Richard-Allan Scientific)
136 as previously described [25]. Frozen eyecups were mounted on a cryostat chuck in an orientation that sections
137 became perpendicular to the retinal plane at the central retina. Eight-µm thick, serial sections were collected from
138 the middle 1/3 of eyecups and used for immunohistochemistry. Immunostaining and imaging procedures were
139 previously described elsewhere [25]. To assess the photoreceptor cell loss, 3 serial sections that contained the
140 central retina were selected and the number of rows of photoreceptor cell nuclei was counted near the center of

141 the retina (300-600 μ m from the optic nerve head; 2 locations/section). One-way ANOVA followed by Tukey's
142 multiple comparison test was used for statistical analyses using GraphPad Prism software. *P* values smaller than
143 0.01 were regarded as statistically significant.

144

145 Retinal sections to assess NPHP1 localization to the connecting cilium were prepared as previously described
146 [25]. Fluorescence intensities were measured using ImageJ/Fiji. Background fluorescence intensity in the vicinity
147 of each connecting cilium was subtracted from the intensity of NPHP1 at the connecting cilium. Two-tailed *t*-test
148 assuming unequal variances was performed for statistical analysis.

149

150 mIMCD-3 cells were obtained from ATCC (#CRL-2123) and cultured in DMEM:F12 Medium (Invitrogen)
151 supplemented with 10% fetal bovine serum (Sigma), 100 units/mL of penicillin, and 100 μ g/mL of streptomycin
152 (Invitrogen). HA-tagged NPHP1 expression vectors were transfected to mIMCD-3 cells using FuGENE HD
153 (Promega) following the manufacturer's instruction. Immunostaining and imaging procedures are described in
154 [37].

155

156 **Electroretinogram (ERG)**

157 Mice were dark-adapted overnight before ERG recording. Under dim red light illumination, mice were
158 anesthetized by intraperitoneal injection of a ketamine/xylazine mixture (87.5 mg/kg and 12.5 mg/kg,
159 respectively), and pupils were dilated with 1% tropicamide ophthalmic solution (Akorn) for 2-3 minutes. Mice
160 were placed on a Celeris D430 rodent ERG testing system (Diagnosys) with its heater on to maintain animals'
161 body temperature. After applying GenTeal Tears Lubricant Eye Gel (Alcon), light-guide electrodes were
162 positioned on both eyes. For dim light scotopic ERG, responses were measured with 15 flashes of 0.01 cd·sec/m²
163 stimulating light (color temperature: 6500K). Dark-adapted Standard Combined Response (SCR) was measured
164 with 15 flashes of 3.0 cd·sec/m² stimulating light (color temperature: 6500K). For photopic ERG, mice were light-
165 adapted for 10 minutes (background light; 9.0 cd·sec/m²) and responses were measured with 15 flashes of 3.0
166 cd·sec/m² white light (6500K). After recording, animals were allowed to recover on a heating pad.

167

168 **RNA extraction and reverse transcription (RT)-PCR**

169 Tissue collection and RNA extraction procedures were described previously [25]. *Nphp1* cDNA fragments
170 between exons 2 and 11 were PCR-amplified using Universe High-Fidelity Hot Start DNA polymerase (Bimake)
171 and two primers (F1-mNPHP1-RT and R1-mNPHP1-RT) listed in **Table 1**. PCR products were directly sequenced
172 by Sanger sequencing using the F1-mNPHP1-RT primer. Band intensities were measured using the Image Lab
173 software (Bio-Rad).

174

175 **Immunoprecipitation**

176 HEK 293T/17 cells were obtained from ATCC (#CRL-11268) and cultured in Dulbecco's Modified Eagle's
177 Medium (DMEM; Invitrogen) supplemented with 10% fetal bovine serum (Sigma), 100 units/mL of penicillin,
178 and 100 µg/mL of streptomycin (Invitrogen). GFP-NPHP2 and GFP-NPHP5 expression vectors were transiently
179 transfected to 293T/17 cells together with pCS2FLAG empty vectors (as a control) or pCS2FLAG-NPHP1
180 variants using FuGENE HD (Promega), following the manufacturer's instruction. Protein extracts were prepared
181 and subjected to immunoprecipitation with anti-FLAG M2 magnetic beads (Sigma) as previously described [25].
182 SDS-PAGE and immunoblotting were performed as described above.

183

184 Results

185 Mislocalization of inner segment plasma membrane-associated proteins in *Nphp1*^{gt/gt} 186 retinas

187 To test the requirement of NPHP1 for compartmentalized protein localization in photoreceptors, we probed the
188 localization of various IS and OS resident proteins in *Nphp1*^{gt/gt} mouse retinas. Our prior study showed that IS
189 plasma membrane proteins STX3, STXBP1, SNAP25, and IMPG2 were the most susceptible to mislocalization
190 in CEP290-deficient photoreceptors [25]. Therefore, we focused our efforts on these proteins. In normal
191 photoreceptors, these proteins were strictly restricted to the IS (hereafter our use of the term IS encompasses all
192 parts of photoreceptors except the OS) (**Fig 1**). In 18-day old *Nphp1*^{gt/gt} mutants, however, all of these proteins
193 showed significant mislocalization to the OS (**Fig 1A-D**; see **Fig 1E** for quantification). STXBP1 showed the most
194 severe mislocalization with approximately 1/3 of proteins mislocalized to the OS. Consistent with the previous
195 finding [22], mislocalization of RHO to the IS was relatively mild in *Nphp1*^{gt/gt} mutants and no mislocalization
196 was detected with other OS resident proteins examined (PRPH2, ROM1, ABCA4, and PDE6B) (**Fig 1 and S3**
197 **Fig**).

198

199 **Fig 1. Temporary impairment of protein confinement and retinal degeneration in *Nphp1*^{gt/gt} mice.**

200 (A-D) Transient mislocalization of STX3 (A), STXBP1 (B), SNAP25 (C), and IMPG2 (D) in *Nphp1*^{gt/gt} retinas.
201 Retinal sections from *Nphp1*^{+/gt} and *Nphp1*^{gt/gt} mice were stained with STX3, STXBP1, SNAP25, and IMPG2
202 antibodies (green). PRPH2, RHO, ROM1, and ABCA4 (red) were labeled as a marker of the OS. Merged images
203 are shown on the left. DAPI (blue) was used to counterstain the nuclei. Scale bar denotes 50 μ m. IS: inner segment,
204 ONL: outer nuclear layer, OPL: outer plexiform layer. OS: outer segment.

205 (E) Quantification of IS membrane protein mislocalization to the OS. Depicted are the ratios of integrated
206 fluorescence intensities in the OS relative to the photoreceptor cell layer. Mean \pm standard deviation (SD; error
207 bars) is marked by horizontal lines (n=3 mice; 2 sections/mouse and 3 areas/section). Asterisks indicate statistical
208 significance (one-way ANOVA followed by Tukey's multiple comparison test; $p < 0.01$).

209 (F) Temporary retinal degeneration in *Nphp1^{gt/gt}* retinas. The number of rows of photoreceptor cell nuclei was
210 counted in *Nphp1^{+/gt}* and *Nphp1^{gt/gt}* mice at the central retina (n=4 mice; 3 sections/mouse; 2 locations/section).
211 Mean \pm SD is shown. Asterisks indicate statistical significance (one-way ANOVA; $p < 0.01$).

212

213 We then examined whether IS membrane proteins progressively accumulated in the OS as in *Cep290* mutant
214 retinas [25]. To our surprise, localization of all proteins examined (STX3, STXBP1, SNAP25, and IMPG2) was
215 significantly improved in 30-day old *Nphp1^{gt/gt}* mutants and only a subset of photoreceptors displayed
216 mislocalization (P30 in **Fig 1A-E**). Localization of these proteins was even further improved by P60 and became
217 indistinguishable from normal controls by P120. Mislocalization of RHO, PRPH2, ROM1, ABCA4, and PDE6B
218 was not detected after P30 (**Fig 1 and S3 Fig**).

219

220 To test whether loss of NPHP1 more preferentially affects cone OS proteins, we examined the localization of
221 OPN1MW (cone opsin) and GNAT2 (cone transducin α) in *Nphp1^{gt/gt}* mutants (**Fig 2**). In 18-day old *Nphp1^{gt/gt}*
222 mice, cone OSs appeared to be short and disorganized. OPN1MW mostly localized to the OS but a small
223 proportion was found mislocalized to the IS (**Fig 2A and C**). In contrast, localization of GNAT2 was not altered
224 in *Nphp1^{gt/gt}* retinas (**Fig 2B and C**). At P30 and P120, cone OSs appeared to be normal in length and shape, and
225 no mislocalization of cone OS proteins was detected.

226

227 **Fig 2. Localization of cone OS proteins in *Nphp1^{gt/gt}* retinas.**

228 (A-B) Cone OS proteins, OPN1MW (A) and GNAT2 (B), were immunostained in *Nphp1^{+/gt}* and *Nphp1^{gt/gt}* retinal
229 sections. Mild mislocalization of OPN1MW was observed at P18 but not at P30 in *Nphp1^{gt/gt}* retinas. Scale bar
230 denotes 50 μ m.

231 (C) Quantification of cone OS protein mislocalization to the IS. Others are the same as in Fig 1E.

232

233 **Retinal degeneration in *Nphp1^{gt/gt}* mice**

234 We examined photoreceptor degeneration in *Nphp1^{gt/gt}* mutants. To this end, we counted the number of rows of
235 photoreceptor cell nuclei at the central retina (300-600 μ m from the optic nerve head). Consistent with the previous

236 finding [22], there was a slight loss (~1 row) of photoreceptor cells by P18 (mean \pm SD: 12.7 ± 0.7 in *Nphp1*^{+/gt}
237 vs. 11.6 ± 0.9 in *Nphp1*^{gt/gt}; $p < 0.01$; n=4) (**Fig 1F**). Thinning of the outer nuclear layer became more obvious and
238 3-4 rows of photoreceptors were lost by P30 (mean \pm SD: 9.1 ± 0.9 at P30; $p < 0.01$ compared with *Nphp1*^{gt/gt} at
239 P18; n=4). However, retinal degeneration stopped thereafter and ~70% of photoreceptors were retained until 4
240 months of age (the last time point examined) in *Nphp1*^{gt/gt} mice (8.8 ± 0.9 at P60 and 8.6 ± 0.8 at P120; n=4) (**Fig**
241 **1F**).

242

243 **Normal retinal functions in *Nphp1*^{gt/gt} mice**

244 We next examined whether *Nphp1*^{gt/gt} mouse retinas were functionally normal despite the initial protein
245 mislocalization and partial loss of photoreceptors (**Fig 3**). In both scotopic and photopic conditions,
246 electroretinogram (ERG) of 2-month old *Nphp1*^{gt/gt} mice was comparable to that of control animals (n=4). These
247 data indicate that both rods and cones recover from the initial protein confinement defect and become fully
248 functional in *Nphp1*^{gt/gt} mice.

249

250 **Fig 3. *Nphp1*^{gt/gt} mouse retinas respond normally to light.**

251 Scotopic (A and B) and photopic (C) ERG recordings of 2-month old *Nphp1*^{+/gt} and *Nphp1*^{gt/gt} mice are shown.
252 Stimulus light intensities are shown on the left.

253

254 **Production of functional mRNAs from the *Nphp1*^{gt} allele**

255 Spontaneous amelioration of protein mislocalization and temporary retinal degeneration in *Nphp1*^{gt/gt} mice sharply
256 contrast with the severe retinal degeneration phenotype observed in *Nphp1*^{del20/del20} mice [5]. To gain insights into
257 the molecular basis of these striking differences, we examined possible expression of normal or mutant variants
258 of NPHP1 in *Nphp1*^{gt/gt} mice. More specifically, we directed our attention to non-canonical mRNA splicing events
259 that could result in the production of functional proteins. Basal exon skipping and nonsense-associated altered
260 splicing are mechanisms, through which cells eliminate nonsense or frameshift mutation-containing exons during
261 the pre-mRNA splicing. The resulting mRNAs maintain the reading frame of the gene and produce near-full-

262 length proteins [45-50]. Neighboring exon(s) may be skipped as well if omitting the mutated exon alone does not
263 prevent frameshift. These non-canonical splicing events have been reported in the human *CEP290* gene and
264 account for the unexpectedly mild phenotypes observed in certain *CEP290*-LCA patients [47-50]. We recently
265 showed that nonsense-associated altered splicing also occurs in a mouse model *CEP290*-LCA [25]. The *Nphp1^{gt}*
266 allele was generated by an insertion of a gene-trap into exon 4 (**S1 Fig**) [22], and we examined whether altered
267 splicing occurred in *Nphp1^{gt/gt}* mice.

268

269 To assess exon skipping, RNAs were extracted from 1.5-month old *Nphp1^{+/+}* and *Nphp1^{gt/gt}* mouse eyes, and
270 cDNA fragments were PCR amplified using primers specific to *Nphp1* exons 2 and 11 (forward and reverse
271 primers, respectively). In *Nphp1^{+/+}* mice, a single PCR product containing all exons between exons 2 and 11 was
272 amplified (991 bp; based on the transcript ID ENSMUST00000028857.13) (**Fig 4A**; left), suggesting no basal
273 exon skipping. A slightly smaller fragment (805 bp) was amplified from *Nphp1^{gt/gt}* mice. Sequence analyses of
274 these PCR products revealed that the 805-bp fragment contained *Nphp1* coding sequences but lacked exons 3 and
275 4 as well as the gene-trap (**Fig 4B**). These data indicate that the entire gene-trap plus *Nphp1* exons 3 and 4 were
276 skipped during pre-mRNA splicing. *Nphp1* exons 3 and 4 are 61 bp and 125 bp long, respectively. Skipping of
277 these two exons results in an in-frame deletion of 62 amino acids (aa; from Cys49 to Lys110 (p.C49_K110del))
278 within the N-terminal coiled-coil domain (**Fig 4C**). These data demonstrate that nonsense-associated altered
279 splicing does occur in *Nphp1^{gt}* transcripts.

280

281 **Fig 4. A small quantity of functional mRNA is produced from the *Nphp1^{gt}* allele via nonsense-associated**
282 **altered splicing.**

283 (A) *Nphp1* RT-PCR data from *Nphp1^{+/+}*, *Nphp1^{gt/gt}*, and *Nphp1^{+/gt}* retinas. Black and red arrowheads indicate
284 PCR products from the wild-type and the *Nphp1^{gt}* allele, respectively. Each animal's *Nphp1* genotype is shown at
285 the top. Locations of DNA size markers are shown on the left.

286 (B) Chromatogram of RT-PCR product sequencing reactions around exon-exon junctions. Vertical dotted lines
287 indicate exon-exon junctions.

288 (C) Schematic representation of NPHP1 protein products encoded by wild-type and *Nphp1^{gt}* alleles. Major
289 structural domains are depicted (Coil: coiled-coil domain; E: Glu-rich domain; SH3: SH3 domain; NHD:
290 nephrocystin homology domain). Amino acid positions are shown below full-length NPHP1 and based on the
291 translated amino acid sequence of BC118953.

292

293 We noticed that the band intensity of the 805-bp fragment was significantly lower than that of wild-type fragments
294 (**Fig 4A**; left). To better assess the quantity of *Nphp1^{gt}* mRNAs produced by nonsense-associated altered splicing,
295 we performed PCR using cDNAs from *Nphp1^{+/gt}* heterozygous mice and stopped PCR amplification after 30
296 cycles (i.e., before saturation) (**Fig 4A**; right). Using wild-type bands as an internal control, densitometric analysis
297 of the PCR products indicated that the quantity of *Nphp1^{gt}* altered splicing products was less than 10% of wild-
298 type mRNAs (mean \pm SD: $6.3 \pm 1.0\%$; n=4). To test whether the nonsense-associated altered splicing is an age-
299 dependent phenomenon and underlies the temporary retinal phenotypes, RNAs were extracted from 10-day old
300 *Nphp1^{+/+}*, *Nphp1^{+/gt}*, and *Nphp1^{gt/gt}* mouse eyes, and RT-PCR was conducted using the same PCR primers. RT-
301 PCR results from young animals were similar to those of adult mice (**S4 Fig**), indicating that nonsense-associated
302 altered splicing occurs similarly in both developing and matured retinas.

303

304 **Expression and localization of the NPHP1 deletion mutant encoded by the *Nphp1^{gt}* allele**

306 We characterized the NPHP1 mutant protein encoded by the *Nphp1^{gt}* allele (hereafter NPHP1 $\Delta(49-110)$). With
307 the antibodies available to us, we were not able to detect endogenous NPHP1 convincingly in the retina by
308 immunoblotting. Therefore, we used protein extracts from testes, in which ciliary proteins were enriched (**Fig**
309 **5A**). While full-length NPHP1 with a calculated molecular weight of 77 kDa was readily detected in *Nphp1^{+/+}*
310 testes (red arrowhead), we were not able to detect any unique protein band in *Nphp1^{gt/gt}* testes.

311

312 **Fig 5. Expression and localization of NPHP1 $\Delta(49-110)$ deletion mutants.**

313 (A) Immunoblotting of NPHP1 (red arrowhead) in *Nphp1*^{+/+} and *Nphp1*^{gt/gt} mouse testes. Fifty µg of proteins were
314 loaded per lane. β-actin was used as a loading control.

315 (B) Localization of NPHP1 Δ(49-110) to the connecting cilium. Connecting cilia are marked by GT335
316 polyglutamylated antibodies (red). NPHP1 immunoreactivity (green) is detected at the connecting cilium (red
317 arrowheads) in both *Nphp1*^{+/+} and *Nphp1*^{gt/gt} retinas but significantly reduced in *Nphp1*^{gt/gt} retinas. White
318 arrowheads indicate connecting cilia with no NPHP1 immunoreactivity. Open arrowheads denote cross-reacting
319 protein(s) around the basal body. Scale bar represents 1 µm.

320 (C) Quantification of NPHP1 immunofluorescence intensities (in arbitrary units; AU) at the connecting cilium.
321 Mean ± SD is marked by horizontal lines (n=30; 2 mice). Asterisks indicate statistical significance (t-test; $p <$
322 0.001).

323 (D) Expression of HA-tagged NPHP1 and NPHP1 Δ(49-110) in transiently transfected 293T/17 cells.

324 (E) Localization of NPHP1 Δ(49-110) to the transition zone in mIMCD-3 cells. HA-NPHP1 and HA-NPHP1
325 Δ(49-110) were transiently transfected to mIMCD-3 cells and their localization was probed with anti-HA
326 antibodies (green; white arrowhead). ARL13B (red) was labeled as a marker of primary cilia. Scale bar represents
327 5 µm.

328

329 We then examined the localization of NPHP1 in the retina by immunohistochemistry (**Fig 5B**). As previously
330 reported [4, 5], NPHP1 was found at the connecting cilium in normal photoreceptor cells (red arrowhead). Signals
331 around the basal body (open arrowhead) were from cross-reacting protein(s). Consistent with the immunoblotting
332 data, NPHP1 immunoreactivity at the connecting cilium was drastically reduced in *Nphp1*^{gt/gt} retinas (**Fig 5B and**
333 **C**). However, low-level immunoreactivity was detected in a subset of cells (**Fig 5B**; red arrowhead), suggesting
334 that NPHP1 Δ(49-110) mutants are expressed and localize to the connecting cilium.

335

336 To confirm the localization of NPHP1 Δ(49-110) to the connecting cilium, we generated expression plasmids
337 encoding the full-length and the deletion mutant form of NPHP1 with an N-terminal HA tag and examined their
338 localization in ciliated mIMCD-3 cells. As shown in **Fig 5D and E**, HA-NPHP1 Δ(49-110) was as efficiently

339 produced as HA-NPHP1 and localized to the transition zone in mIMCD-3 cells. These data indicate that the mutant
340 protein retains its ability to localize to the connecting cilium.

341

342 **NPHP1 Δ(49-110) mutants retain the ability to interact with other NPHP proteins**

343 We then examined whether the 62-aa deletion had any impact on protein-protein interactions of NPHP1. NPHP1
344 is previously shown to interact with AHI1, NPHP2 (also known as INVS), NPHP4, NPHP5 (IQCB1), and NPHP8
345 (RPGRIP1L) [10, 51-54]. Of these, NPHP1 directly binds to AHI1 and NPHP4 via its SH3 domain and the C-
346 terminal 131 residues, respectively [10, 51, 53, 54]. Since these regions are preserved in the NPHP1 Δ(49-110)
347 mutant and sufficient to mediate NPHP1 interactions with AHI1 and NPHP4, we focused our efforts on
348 interactions with NPHP2, NPHP5, and NPHP8. To this end, we transiently transfected FLAG-tagged NPHP1
349 variants (full-length NPHP1, NPHP1 Δ(49-110), and NPHP1 aa242-685) with GFP-tagged NPHP2 and NPHP5,
350 and performed immunoprecipitation (IP) using anti-FLAG antibodies (**Fig 6**). For NPHP8, endogenous proteins
351 were probed. As shown in **Fig 6**, both NPHP1 Δ(49-110) and NPHP1 aa242-685 were able to pull down all three
352 NPHP proteins, indicating that the C-terminal nephrocystin homology domain (NHD) alone was sufficient to
353 interact with these proteins either directly or indirectly. These data show that the NPHP1 Δ(49-110) mutant retains
354 most, if not all, of its protein-protein interaction capabilities.

355

356 **Fig 6. Interaction of NPHP1 Δ(49-110) with other NPHP proteins.**

357 Expression vectors of FLAG-tagged NPHP1 (full-length), NPHP1 Δ(49-110), and NPHP1 aa242-685 were co-
358 transfected with either pEGFP-NPHP2 (A) or pEGFP-NPHP5 (B) to 293T/17 cells, and protein extracts were
359 subjected to immunoprecipitation (IP) with anti-FLAG antibodies. Empty vectors were used as a negative control
360 (CTRL). For NPHP8 (C), endogenous NPHP8 was probed.

361

362 ***Cep290* genetically interacts with *Nphp1* and modifies retinal phenotypes in**
363 ***Nphp1^{gt/gt}* mice**

364 Finally, we tested whether additional mutations in other ciliary gate-related genes could modify the severity of
365 retinal degeneration in *Nphp1*^{gt/gt} mice. To this end, we crossed *Nphp1*^{gt/gt} mice to *Cep290*^{fl/fl}; *iCre75* mice [25, 30,
366 31] and compared protein mislocalization and retinal degeneration phenotypes in *Nphp1*^{gt/gt}; *Cep290*^{+/+}; *iCre75* and
367 *Nphp1*^{gt/gt}; *Cep290*^{+/fl}; *iCre75* animals: all animals analyzed in this study were *iCre75* hemizygotes and *iCre75*
368 genotype is omitted for brevity. At 1 month of age, mislocalization of IS plasma membrane proteins STX3,
369 STXBP1, and SNAP25 was significantly increased in *Nphp1*^{gt/gt}; *Cep290*^{+/fl} mice compared with that in
370 *Nphp1*^{gt/gt}; *Cep290*^{+/+} mice (Fig 7). RHO mislocalization was also detected in *Nphp1*^{gt/gt}; *Cep290*^{+/fl} mice, but it was
371 relatively mild compared to that of IS membrane proteins. Consistent with the increased protein mislocalization,
372 reduction of the outer nuclear layer was evident in *Nphp1*^{gt/gt}; *Cep290*^{+/fl} mice. At 2 months of age, when
373 *Nphp1*^{gt/gt}; *Cep290*^{+/+} mice exhibited no mislocalization and no degeneration, *Nphp1*^{gt/gt}; *Cep290*^{+/fl} mice exhibited
374 severe retinal degeneration with only 3-5 rows of photoreceptor cell nuclei remaining. In *Nphp1*^{gt/gt}; *Cep290*^{fl/fl}
375 double mutants, more than 90% of photoreceptors were lost by P30, which is faster than what we observed in
376 *Cep290*^{fl/fl} single mutants using the same *Cre* driver [25]. These data indicate that *Nphp1* and *Cep290* genetically
377 interact and that reduction of *Cep290* gene dose exacerbates protein confinement defects and causes continuous
378 retinal degeneration in *Nphp1*^{gt/gt} mice.

379

380 **Fig 7. Genetic interaction of *Nphp1* with *Cep290*.**

381 Mislocalization of STX3 (A), STXBP1 (B), and SNAP25 (C) in *Nphp*^{gt/gt}; *Cep290*^{+/+}, *Nphp*^{gt/gt}; *Cep290*^{+/fl}, and
382 *Nphp*^{gt/gt}; *Cep290*^{fl/fl} retinas (green). PRPH2, RHO, and ROM1 (red) were labeled to mark the OS. The ratio of
383 mislocalized proteins was quantified as in Fig 1 and depicted on the right. Mean \pm SD is marked by horizontal
384 lines (n=3 mice; 2 sections/mouse and 3 areas/section). Asterisks indicate statistical significance (one-way
385 ANOVA followed by Tukey's multiple comparison test; $p < 0.01$).

386

387 Discussion

388 In this work, we characterize retinal degeneration in a mouse model of NPHP1 and demonstrate the requirement
389 of NPHP1 for compartmentalized protein localization in photoreceptors. The mutant allele in the *Nphp1^{gt}* model
390 is a hypomorph rather than a null because of the production of a small number of functional mRNAs derived from
391 nonsense-associated altered splicing. The resulting mRNAs encode a near-full-length protein with a 62-aa in-
392 frame deletion. The mutant protein appears to retain most, if not all, functions of the full-length protein, as it
393 correctly localizes to the ciliary transition zone and interacts with its known binding partners. However, the
394 quantity of the functional mRNAs produced by altered splicing is very low (less than 10% of wild type), and the
395 protein products are undetectable or barely detectable in the testis and the retina with the reagents available to us.
396 Although we were not able to detect the mutant protein in the testis, it is noteworthy that all *Nphp1^{gt/gt}* males
397 (n=12) used for breeding produced offspring with normal litter size (5-12 pups/litter). This is contrary to the
398 sterility of *Nphp1^{del20/del20}* males [21]. Therefore, our data suggest that the *Nphp1^{gt}* allele is a hypomorph and that
399 the phenotypic differences between the two NPHP1 mouse models are due to a difference in the residual activities
400 of the two mutant alleles rather than genetic backgrounds.

401

402 Our study shows that NPHP1 is involved in membrane protein confinement at the connecting cilium. In
403 developing *Nphp1^{gt/gt}* retinas, confinement of IS plasma membrane proteins is compromised, leading to an
404 infiltration of IS membrane proteins into the OS. Among the OS proteins examined, only opsins (RHO and
405 OPN1MW) showed mislocalization to the IS and the degree of mislocalization was relatively mild compared to
406 that of IS plasma membrane proteins. This phenotype is very similar to what is observed in *Cep290^{fl/fl}* mice [25]. It
407 also should be noted that, despite more severe RHO mislocalization and faster degeneration, IS membrane protein
408 mislocalization does not occur in *Ift88* mutants (**S5 Fig**). This suggests that IS membrane protein mislocalization
409 is not a consequence of the degenerative process occurring in dying cells. Therefore, although it has been
410 examined in only two disease models thus far, our findings are consistent with the idea that accumulation of IS
411 membrane proteins in the OS is a common pathomechanism of retinal degenerations associated with ciliary gate
412 defects [3]. Further investigation is needed to validate this idea in other ciliary gate-related retinal degenerations.

413 It is also noteworthy that although Bardet-Biedl syndrome (BBS) proteins are not part of the ciliary gate complex,
414 retinal degeneration in BBS shares the same disease mechanism [38, 55, 56]. Future studies should be directed to
415 how this molecular phenotype leads to the death of photoreceptor cells.

416

417 Interestingly, however, the requirement of NPHP1 in photoreceptors is developmental stage dependent. In mice,
418 the connecting cilium assembles at P3-5 and the OS develops afterward until P18-20 [57, 58]. Protein
419 mislocalization occurs in *Nphp1^{gt/gt}* retinas when OSs are actively elongating, but normal distribution patterns are
420 restored after P18. Some photoreceptors die during this period, but retinal degeneration stops as the protein
421 confinement defect is ameliorated. Retinal functions and anatomy are normal in adult *Nphp1^{gt/gt}* mice except ~30%
422 thinner ONL due to the earlier loss of photoreceptors. RT-PCR data indicate that nonsense-associated altered
423 splicing of *Nphp1^{gt}* pre-mRNAs occurs in not only fully matured but also developing retinas. Therefore, age-
424 dependent differences in altered splicing are not likely a contributing factor. One speculation is that, although
425 ciliary gate functions are essential throughout the life of photoreceptors, more vigorous NPHP1 activities might
426 be needed when OSs are rapidly elongating compared to when the OS elongation is completed.

427

428 Our study suggests that additional mutations in other ciliary gate-related genes may affect the penetrance of
429 retinopathy in human NPHP1 patients. As mentioned in the Introduction, only 6-10% of NPHP1 patients manifest
430 retinal anomalies [19, 20, 59]. The most frequent mutations in human *NPHP1*, found in 65-80% of NPHP1 patients,
431 are large (~250 kb) homozygous deletions that eliminate the majority of *NPHP1* exons [16-18, 60]. Since these
432 mutations are expected to be null, NPHP1 does not appear to be essential for photoreceptor health in humans. A
433 previous study showed that removal of one allele of *Ahi1*, which encodes a component of the ciliary gate complex
434 [10], significantly increases RHO mislocalization and accelerates retinal degeneration in *Nphp1^{gt/gt}* mice [22]. In
435 the present work, we show that reducing the gene dose of *Cep290* in *Nphp1^{gt/gt}* mice exacerbates protein
436 mislocalization and causes retinal degeneration that continues in mature retinas. These findings suggest that
437 *NPHP1* genetically interacts with other ciliary gate-related genes and that the manifestation of retinopathy in
438 NPHP1 patients may be affected by the presence of additional mutations in those genes.

439

440 Our study also suggests that mutation-induced non-canonical splicing might be more common than what has been
441 appreciated. As mentioned above, some *CEP290*-LCA patients exhibit relatively mild phenotypes despite the
442 presence of truncation mutations that should eliminate a large proportion of the protein [47-50]. The unexpectedly
443 mild phenotypes are due to the production of near-full-length proteins derived from non-canonical mRNA splicing
444 that skips exons with truncating mutations. One of the interesting features of inherited retinal degenerations is the
445 wide spectrum of phenotypic severity despite mutations in the same gene [20, 61-67]. Although some of these
446 variations can be explained by disease-causing mutations *per se* (e.g. missense mutations that partly reduce protein
447 activities) and genetic modifiers, nonsense-associated altered splicing may contribute to the variation and underlie
448 the mild end of the phenotypic spectrum of disease.

449

450 Finally, our study urges a more thorough investigation of mRNAs produced in mutant animals. When loss-of-
451 function animal models are generated, inducing frameshift is a frequently used strategy. For example, CRISPR-
452 based gene knockout approaches utilize the tendency of introducing indels at double-strand breaks, which results
453 in a frameshift. In more conventional recombination-based approaches, exons, deletion of which causes frameshift,
454 are preferentially selected when designing targeting vectors. Accumulating evidence indicates that exons
455 containing premature termination codons are often skipped as a compensatory mechanism to cope with induced
456 mutations [68-70]. Our results show that gene-traps can be skipped as well during splicing. Therefore, a thorough
457 investigation of mRNAs produced from mutant alleles is warranted before beginning extensive studies and making
458 conclusions without knowing the precise consequences of the mutation.

459

460

461 **Conclusions**

462 Our study shows that NPHP1 is required to maintain compartmentalized protein localization during the
463 photoreceptor terminal differentiation, particularly to prevent infiltration of IS plasma membrane proteins into the
464 OS. However, this requirement is developmental stage-dependent, and NPHP1 becomes less crucial as the OS
465 elongation is completed. Retinal degeneration occurs when NPHP1 deficiency causes protein mislocalization but
466 stops as normal localization patterns are restored. These findings suggest that accumulation of IS membrane
467 proteins in the OS is part of the disease mechanisms underlying the *NPHP1*-associated retinopathy. Our study
468 further shows that reduction of *Cep290* gene dose exacerbates protein confinement defects and retinal
469 degeneration in *Nphp1* mutants. These findings suggest that additional mutations in other ciliary gate-related genes
470 may influence the penetrance of retinopathy in human NPHP1 patients.

471

472

473

474 **Financial disclosure**

475 No author has a financial or proprietary interest in any material or method enclosed.

476

477

478

479 **Acknowledgments**

480 We thank Drs. Val C. Sheffield and William Y. Tsang for the gifts of pEGFP-NPHP2 and pEGFP-NPHP5. This
481 work was supported by National Institutes of Health grants R01-EY022616 and R21-EY027431 (to S.S.), National
482 Institutes of Health Center Support grant P30-EY025580 (to the University of Iowa), and Research to Prevent
483 Blindness Unrestricted Grant (to the Department of Ophthalmology and Visual Sciences, University of Iowa).

484

485 References

486 1. Pearring JN, Salinas RY, Baker SA, Arshavsky VY. Protein sorting, targeting and trafficking in
487 photoreceptor cells. *Progress in retinal and eye research*. 2013;36:24-51. doi: 10.1016/j.preteyeres.2013.03.002.
488 PubMed PMID: 23562855; PubMed Central PMCID: PMC3759535.

489 2. Baehr W, Hanke-Gogokhia C, Sharif A, Reed M, Dahl T, Frederick JM, et al. Insights into photoreceptor
490 ciliogenesis revealed by animal models. *Progress in retinal and eye research*. 2019;71:26-56. Epub 2018/12/28.
491 doi: 10.1016/j.preteyeres.2018.12.004. PubMed PMID: 30590118; PubMed Central PMCID: PMCPMC6707082.

492 3. Seo S, Datta P. Photoreceptor outer segment as a sink for membrane proteins: hypothesis and implications
493 in retinal ciliopathies. *Hum Mol Genet*. 2017;26(R1):R75-R82. doi: 10.1093/hmg/ddx163. PubMed PMID:
494 28453661; PubMed Central PMCID: PMCPMC5886464.

495 4. Fliegauf M, Horvath J, von Schnakenburg C, Olbrich H, Muller D, Thumfart J, et al. Nephrocystin
496 specifically localizes to the transition zone of renal and respiratory cilia and photoreceptor connecting cilia. *J Am
497 Soc Nephrol*. 2006;17(9):2424-33. Epub 2006/08/04. doi: 10.1681/ASN.2005121351. PubMed PMID: 16885411.

498 5. Jiang ST, Chiou YY, Wang E, Chien YL, Ho HH, Tsai FJ, et al. Essential role of nephrocystin in
499 photoreceptor intraflagellar transport in mouse. *Hum Mol Genet*. 2009;18(9):1566-77. Epub 2009/02/12. doi:
500 10.1093/hmg/ddp068. PubMed PMID: 19208653.

501 6. Schermer B, Hopker K, Omran H, Ghenoiu C, Fliegauf M, Fekete A, et al. Phosphorylation by casein
502 kinase 2 induces PACS-1 binding of nephrocystin and targeting to cilia. *EMBO J*. 2005;24(24):4415-24. Epub
503 2005/11/26. doi: 10.1038/sj.emboj.7600885. PubMed PMID: 16308564; PubMed Central PMCID:
504 PMCPMC1356326.

505 7. Seeger-Nukpezah T, Liebau MC, Hopker K, Lamkemeyer T, Benzing T, Golemis EA, et al. The
506 centrosomal kinase Plk1 localizes to the transition zone of primary cilia and induces phosphorylation of
507 nephrocystin-1. *PLoS One*. 2012;7(6):e38838. Epub 2012/06/16. doi: 10.1371/journal.pone.0038838. PubMed
508 PMID: 22701722; PubMed Central PMCID: PMCPMC3372538.

509 8. Garcia-Gonzalo FR, Corbit KC, Sirerol-Piquer MS, Ramaswami G, Otto EA, Noriega TR, et al. A
510 transition zone complex regulates mammalian ciliogenesis and ciliary membrane composition. *Nature genetics*.
511 2011;43(8):776-84. Epub 2011/07/05. doi: 10.1038/ng.891. PubMed PMID: 21725307; PubMed Central PMCID:
512 PMC3145011.

513 9. Shi X, Garcia G, 3rd, Van De Weghe JC, McGorty R, Pazour GJ, Doherty D, et al. Super-resolution
514 microscopy reveals that disruption of ciliary transition-zone architecture causes Joubert syndrome. *Nat Cell Biol*.

515 2017;19(10):1178-88. Epub 2017/08/29. doi: 10.1038/ncb3599. PubMed PMID: 28846093; PubMed Central
516 PMCID: PMCPMC5695680.

517 10. Sang L, Miller JJ, Corbit KC, Giles RH, Brauer MJ, Otto EA, et al. Mapping the NPHP-JBTS-MKS
518 protein network reveals ciliopathy disease genes and pathways. *Cell*. 2011;145(4):513-28. Epub 2011/05/14. doi:
519 10.1016/j.cell.2011.04.019. PubMed PMID: 21565611.

520 11. Williams CL, Li C, Kida K, Inglis PN, Mohan S, Semenec L, et al. MKS and NPHP modules cooperate
521 to establish basal body/transition zone membrane associations and ciliary gate function during ciliogenesis. *The
522 Journal of cell biology*. 2011;192(6):1023-41. Epub 2011/03/23. doi: 10.1083/jcb.201012116. PubMed PMID:
523 21422230; PubMed Central PMCID: PMC3063147.

524 12. Garcia-Gonzalo FR, Reiter JF. Scoring a backstage pass: mechanisms of ciliogenesis and ciliary access.
525 *J Cell Biol*. 2012;197(6):697-709. Epub 2012/06/13. doi: 10.1083/jcb.201111146. PubMed PMID: 22689651;
526 PubMed Central PMCID: PMCPMC3373398.

527 13. Garcia-Gonzalo FR, Reiter JF. Open Sesame: How Transition Fibers and the Transition Zone Control
528 Ciliary Composition. *Cold Spring Harb Perspect Biol*. 2017;9(2):10.1101/cshperspect.a028134. doi:
529 10.1101/cshperspect.a028134. PubMed PMID: 27770015.

530 14. Hildebrandt F, Benzing T, Katsanis N. Ciliopathies. *N Engl J Med*. 2011;364(16):1533-43. doi:
531 10.1056/NEJMra1010172. PubMed PMID: 21506742; PubMed Central PMCID: PMCPMC3640822.

532 15. Reiter JF, Leroux MR. Genes and molecular pathways underpinning ciliopathies. *Nat Rev Mol Cell Biol*.
533 2017;18(9):533-47. Epub 2017/07/13. doi: 10.1038/nrm.2017.60. PubMed PMID: 28698599; PubMed Central
534 PMCID: PMCPMC5851292.

535 16. Konrad M, Saunier S, Heidet L, Silbermann F, Benessy F, Calado J, et al. Large homozygous deletions
536 of the 2q13 region are a major cause of juvenile nephronophthisis. *Hum Mol Genet*. 1996;5(3):367-71. Epub
537 1996/03/01. doi: 10.1093/hmg/5.3.367. PubMed PMID: 8852662.

538 17. Hildebrandt F, Otto E, Rensing C, Nothwang HG, Vollmer M, Adolfs J, et al. A novel gene encoding
539 an SH3 domain protein is mutated in nephronophthisis type 1. *Nat Genet*. 1997;17(2):149-53. Epub 1997/11/05.
540 doi: 10.1038/ng1097-149. PubMed PMID: 9326933.

541 18. Saunier S, Calado J, Heilig R, Silbermann F, Benessy F, Morin G, et al. A novel gene that encodes a
542 protein with a putative src homology 3 domain is a candidate gene for familial juvenile nephronophthisis. *Hum
543 Mol Genet*. 1997;6(13):2317-23. Epub 1998/03/21. doi: 10.1093/hmg/6.13.2317. PubMed PMID: 9361039.

544 19. Hildebrandt F, Attanasio M, Otto E. Nephronophthisis: disease mechanisms of a ciliopathy. *J Am Soc*
545 *Nephrol.* 2009;20(1):23-35. Epub 2009/01/02. doi: 10.1681/ASN.2008050456. PubMed PMID: 19118152;
546 PubMed Central PMCID: PMCPMC2807379.

547 20. Caridi G, Murer L, Bellantuono R, Sorino P, Caringella DA, Gusmano R, et al. Renal-retinal syndromes:
548 association of retinal anomalies and recessive nephronophthisis in patients with homozygous deletion of the NPH1
549 locus. *Am J Kidney Dis.* 1998;32(6):1059-62. Epub 1998/12/18. doi: 10.1016/s0272-6386(98)70083-6. PubMed
550 PMID: 9856524.

551 21. Jiang ST, Chiou YY, Wang E, Lin HK, Lee SP, Lu HY, et al. Targeted disruption of Nphp1 causes male
552 infertility due to defects in the later steps of sperm morphogenesis in mice. *Hum Mol Genet.* 2008;17(21):3368-
553 79. Epub 2008/08/08. doi: 10.1093/hmg/ddn231. PubMed PMID: 18684731.

554 22. Louie CM, Caridi G, Lopes VS, Brancati F, Kispert A, Lancaster MA, et al. AHI1 is required for
555 photoreceptor outer segment development and is a modifier for retinal degeneration in nephronophthisis. *Nat*
556 *Genet.* 2010;42(2):175-80. doi: 10.1038/ng.519. PubMed PMID: 20081859; PubMed Central PMCID:
557 PMCPMC2884967.

558 23. Yee LE, Garcia-Gonzalo FR, Bowie RV, Li C, Kennedy JK, Ashrafi K, et al. Conserved Genetic
559 Interactions between Ciliopathy Complexes Cooperatively Support Ciliogenesis and Ciliary Signaling. *PLoS*
560 *Genet.* 2015;11(11):e1005627. Epub 2015/11/06. doi: 10.1371/journal.pgen.1005627. PubMed PMID: 26540106;
561 PubMed Central PMCID: PMCPMC4635004.

562 24. Rao KN, Zhang W, Li L, Ronquillo C, Baehr W, Khanna H. Ciliopathy-associated protein CEP290
563 modifies the severity of retinal degeneration due to loss of RPGR. *Hum Mol Genet.* 2016;25(10):2005-12. Epub
564 2016/03/05. doi: 10.1093/hmg/ddw075. PubMed PMID: 26936822; PubMed Central PMCID: PMCPMC5062589.

565 25. Datta P, Hendrickson B, Brendalen S, Ruffcorn A, Seo S. The myosin-tail homology domain of
566 centrosomal protein 290 is essential for protein confinement between the inner and outer segments in
567 photoreceptors. *J Biol Chem.* 2019;294(50):19119-36. Epub 2019/11/07. doi: 10.1074/jbc.RA119.009712.
568 PubMed PMID: 31694913; PubMed Central PMCID: PMCPMC6916492.

569 26. den Hollander AI, Koenekoop RK, Yzer S, Lopez I, Arends ML, Voesenek KE, et al. Mutations in the
570 CEP290 (NPHP6) gene are a frequent cause of Leber congenital amaurosis. *American journal of human genetics.*
571 2006;79(3):556-61. Epub 2006/08/16. doi: 10.1086/507318. PubMed PMID: 16909394; PubMed Central PMCID:
572 PMCPMC1559533.

573 27. Sayer JA, Otto EA, O'Toole JF, Nurnberg G, Kennedy MA, Becker C, et al. The centrosomal protein
574 nephrocystin-6 is mutated in Joubert syndrome and activates transcription factor ATF4. *Nat Genet*.
575 2006;38(6):674-81. doi: 10.1038/ng1786. PubMed PMID: 16682973.

576 28. Baala L, Audollent S, Martinovic J, Ozilou C, Babron MC, Sivanandamoorthy S, et al. Pleiotropic effects
577 of CEP290 (NPHP6) mutations extend to Meckel syndrome. *Am J Hum Genet*. 2007;81(1):170-9. PubMed PMID:
578 17564974.

579 29. Cideciyan AV, Aleman TS, Jacobson SG, Khanna H, Sumaroka A, Aguirre GK, et al. Centrosomal-ciliary
580 gene CEP290/NPHP6 mutations result in blindness with unexpected sparing of photoreceptors and visual brain:
581 implications for therapy of Leber congenital amaurosis. *Human mutation*. 2007;28(11):1074-83. Epub 2007/06/08.
582 doi: 10.1002/humu.20565. PubMed PMID: 17554762.

583 30. Lancaster MA, Gopal DJ, Kim J, Saleem SN, Silhavy JL, Louie CM, et al. Defective Wnt-dependent
584 cerebellar midline fusion in a mouse model of Joubert syndrome. *Nat Med*. 2011;17(6):726-31. doi:
585 10.1038/nm.2380. PubMed PMID: 21623382; PubMed Central PMCID: PMCPMC3110639.

586 31. Li S, Chen D, Sauve Y, McCandless J, Chen YJ, Chen CK. Rhodopsin-iCre transgenic mouse line for
587 Cre-mediated rod-specific gene targeting. *Genesis*. 2005;41(2):73-80. doi: 10.1002/gene.20097. PubMed PMID:
588 15682388.

589 32. Turner DL, Weintraub H. Expression of achaete-scute homolog 3 in *Xenopus* embryos converts
590 ectodermal cells to a neural fate. *Genes Dev*. 1994;8(12):1434-47. Epub 1994/06/15. doi: 10.1101/gad.8.12.1434.
591 PubMed PMID: 7926743.

592 33. Gimona M, Vandekerckhove J, Goethals M, Herzog M, Lando Z, Small JV. Beta-actin specific
593 monoclonal antibody. *Cell Motil Cytoskeleton*. 1994;27(2):108-16. Epub 1994/01/01. doi:
594 10.1002/cm.970270203. PubMed PMID: 8162619.

595 34. Datta P, Ruffcorn A, Seo S. Limited time window for retinal gene therapy in a preclinical model of
596 ciliopathy. *Hum Mol Genet*. 2020;29(14):2337-52. Epub 2020/06/23. doi: 10.1093/hmg/ddaa124. PubMed PMID:
597 32568387; PubMed Central PMCID: PMCPMC7424757.

598 35. Illing M, Molday LL, Molday RS. The 220-kDa rim protein of retinal rod outer segments is a member of
599 the ABC transporter superfamily. *J Biol Chem*. 1997;272(15):10303-10. Epub 1997/04/11. PubMed PMID:
600 9092582.

601 36. Molday LL, Rabin AR, Molday RS. ABCR expression in foveal cone photoreceptors and its role in
602 Stargardt macular dystrophy. *Nat Genet.* 2000;25(3):257-8. Epub 2000/07/11. doi: 10.1038/77004. PubMed
603 PMID: 10888868.

604 37. Humbert MC, Weihbrecht K, Searby CC, Li Y, Pope RM, Sheffield VC, et al. ARL13B, PDE6D, and
605 CEP164 form a functional network for INPP5E ciliary targeting. *Proceedings of the National Academy of
606 Sciences of the United States of America.* 2012;109(48):19691-6. Epub 2012/11/15. doi:
607 10.1073/pnas.1210916109. PubMed PMID: 23150559; PubMed Central PMCID: PMC3511769.

608 38. Datta P, Allamargot C, Hudson JS, Andersen EK, Bhattacharai S, Drack AV, et al. Accumulation of non-
609 outer segment proteins in the outer segment underlies photoreceptor degeneration in Bardet-Biedl syndrome. *Proc
610 Natl Acad Sci U S A.* 2015;112(32):E4400-9. doi: 10.1073/pnas.1510111112. PubMed PMID: 26216965.

611 39. Salido EM, Ramamurthy V. Proteoglycan IMPG2 Shapes the Interphotoreceptor Matrix and Modulates
612 Vision. *J Neurosci.* 2020;40(20):4059-72. Epub 2020/04/09. doi: 10.1523/JNEUROSCI.2994-19.2020. PubMed
613 PMID: 32265257; PubMed Central PMCID: PMCPMC7219290.

614 40. Beltran WA, Hammond P, Acland GM, Aguirre GD. A frameshift mutation in RPGR exon ORF15 causes
615 photoreceptor degeneration and inner retina remodeling in a model of X-linked retinitis pigmentosa. *Invest
616 Ophthalmol Vis Sci.* 2006;47(4):1669-81. Epub 2006/03/28. doi: 10.1167/iovs.05-0845. PubMed PMID:
617 16565408.

618 41. Rhee KD, Ruiz A, Duncan JL, Hauswirth WW, Laval MM, Bok D, et al. Molecular and cellular
619 alterations induced by sustained expression of ciliary neurotrophic factor in a mouse model of retinitis pigmentosa.
620 *Invest Ophthalmol Vis Sci.* 2007;48(3):1389-400. Epub 2007/02/28. doi: 10.1167/iovs.06-0677. PubMed PMID:
621 17325188; PubMed Central PMCID: PMCPMC7147570.

622 42. Wolff A, de Nechaud B, Chillet D, Mazarguil H, Desbruyeres E, Audebert S, et al. Distribution of
623 glutamylated alpha and beta-tubulin in mouse tissues using a specific monoclonal antibody, GT335. *Eur J Cell
624 Biol.* 1992;59(2):425-32. Epub 1992/12/01. PubMed PMID: 1493808.

625 43. Sun X, Park JH, Gumerson J, Wu Z, Swaroop A, Qian H, et al. Loss of RPGR glutamylation underlies
626 the pathogenic mechanism of retinal dystrophy caused by TTLL5 mutations. *Proc Natl Acad Sci U S A.*
627 2016;113(21):E2925-34. doi: 10.1073/pnas.1523201113. PubMed PMID: 27162334; PubMed Central PMCID:
628 PMCPMC4889371.

629 44. Molday RS, MacKenzie D. Monoclonal antibodies to rhodopsin: characterization, cross-reactivity, and
630 application as structural probes. *Biochemistry.* 1983;22(3):653-60. Epub 1983/02/01. doi: 10.1021/bi00272a020.
631 PubMed PMID: 6188482.

632 45. Wang J, Chang YF, Hamilton JI, Wilkinson MF. Nonsense-associated altered splicing: a frame-dependent
633 response distinct from nonsense-mediated decay. *Mol Cell*. 2002;10(4):951-7. Epub 2002/11/07. doi:
634 10.1016/s1097-2765(02)00635-4. PubMed PMID: 12419238.

635 46. Sui T, Song Y, Liu Z, Chen M, Deng J, Xu Y, et al. CRISPR-induced exon skipping is dependent on
636 premature termination codon mutations. *Genome Biol*. 2018;19(1):164. Epub 2018/10/20. doi: 10.1186/s13059-
637 018-1532-z. PubMed PMID: 30333044; PubMed Central PMCID: PMCPMC6193291.

638 47. Littink KW, Pott JW, Collin RW, Kroes HY, Verheij JB, Blokland EA, et al. A novel nonsense mutation
639 in CEP290 induces exon skipping and leads to a relatively mild retinal phenotype. *Invest Ophthalmol Vis Sci*.
640 2010;51(7):3646-52. Epub 2010/02/05. doi: 10.1167/iovs.09-5074. PubMed PMID: 20130272.

641 48. Roosing S, Cremers FPM, Riemslag FCC, Zonneveld-Vrieling MN, Talsma HE, Klessens-Godfroy FJM,
642 et al. A Rare Form of Retinal Dystrophy Caused by Hypomorphic Nonsense Mutations in CEP290. *Genes (Basel)*.
643 2017;8(8). Epub 2017/08/23. doi: 10.3390/genes8080208. PubMed PMID: 28829391; PubMed Central PMCID:
644 PMCPMC5575671.

645 49. Drivas TG, Wojno AP, Tucker BA, Stone EM, Bennett J. Basal exon skipping and genetic pleiotropy: A
646 predictive model of disease pathogenesis. *Sci Transl Med*. 2015;7(291):291ra97. Epub 2015/06/13. doi:
647 10.1126/scitranslmed.aaa5370. PubMed PMID: 26062849; PubMed Central PMCID: PMCPMC4486480.

648 50. Barny I, Perrault I, Michel C, Soussan M, Goudin N, Rio M, et al. Basal exon skipping and nonsense-
649 associated altered splicing allows bypassing complete CEP290 loss-of-function in individuals with unusually mild
650 retinal disease. *Hum Mol Genet*. 2018. Epub 2018/05/18. doi: 10.1093/hmg/ddy179. PubMed PMID: 29771326.

651 51. Eley L, Gabrielides C, Adams M, Johnson CA, Hildebrandt F, Sayer JA. Jouberin localizes to collecting
652 ducts and interacts with nephrocystin-1. *Kidney Int*. 2008;74(9):1139-49. Epub 2008/07/18. doi:
653 10.1038/ki.2008.377. PubMed PMID: 18633336.

654 52. Otto EA, Schermer B, Obara T, O'Toole JF, Hiller KS, Mueller AM, et al. Mutations in INVS encoding
655 inversin cause nephronophthisis type 2, linking renal cystic disease to the function of primary cilia and left-right
656 axis determination. *Nat Genet*. 2003;34(4):413-20. Epub 2003/07/23. doi: 10.1038/ng1217. PubMed PMID:
657 12872123; PubMed Central PMCID: PMCPMC3732175.

658 53. Mollet G, Salomon R, Gribouval O, Silbermann F, Bacq D, Landthaler G, et al. The gene mutated in
659 juvenile nephronophthisis type 4 encodes a novel protein that interacts with nephrocystin. *Nat Genet*.
660 2002;32(2):300-5. Epub 2002/09/24. doi: 10.1038/ng996. PubMed PMID: 12244321.

661 54. Mollet G, Silbermann F, Delous M, Salomon R, Antignac C, Saunier S. Characterization of the
662 nephrocystin/nephrocystin-4 complex and subcellular localization of nephrocystin-4 to primary cilia and
663 centrosomes. *Hum Mol Genet*. 2005;14(5):645-56. Epub 2005/01/22. doi: 10.1093/hmg/ddi061. PubMed PMID:
664 15661758.

665 55. Hsu Y, Garrison JE, Kim G, Schmitz AR, Searby CC, Zhang Q, et al. BBSome function is required for
666 both the morphogenesis and maintenance of the photoreceptor outer segment. *PLoS Genet*. 2017;13(10):e1007057.
667 doi: 10.1371/journal.pgen.1007057. PubMed PMID: 29049287; PubMed Central PMCID: PMCPMC5663628.

668 56. Dilan TL, Singh RK, Saravanan T, Moye A, Goldberg AFX, Stoilov P, et al. Bardet-Biedl syndrome-8
669 (BBS8) protein is crucial for the development of outer segments in photoreceptor neurons. *Hum Mol Genet*.
670 2018;27(2):283-94. Epub 2017/11/11. doi: 10.1093/hmg/ddx399. PubMed PMID: 29126234; PubMed Central
671 PMCID: PMCPMC5886228.

672 57. Sedmak T, Wolfrum U. Intraflagellar transport proteins in ciliogenesis of photoreceptor cells. *Biol Cell*.
673 2011;103(10):449-66. doi: 10.1042/BC20110034. PubMed PMID: 21732910.

674 58. Caley DW, Johnson C, Liebelt RA. The postnatal development of the retina in the normal and rodless
675 CBA mouse: a light and electron microscopic study. *Am J Anat*. 1972;133(2):179-212. Epub 1972/02/01. doi:
676 10.1002/aja.1001330205. PubMed PMID: 5009246.

677 59. Hildebrandt F, Zhou W. Nephronophthisis-associated ciliopathies. *J Am Soc Nephrol*. 2007;18(6):1855-
678 71. Epub 2007/05/22. doi: 10.1681/ASN.2006121344. PubMed PMID: 17513324.

679 60. Saunier S, Calado J, Benessy F, Silbermann F, Heilig R, Weissenbach J, et al. Characterization of the
680 NPHP1 locus: mutational mechanism involved in deletions in familial juvenile nephronophthisis. *Am J Hum
681 Genet*. 2000;66(3):778-89. Epub 2000/03/11. doi: 10.1086/302819. PubMed PMID: 10712196; PubMed Central
682 PMCID: PMCPMC1288163.

683 61. Coppieters F, Lefever S, Leroy BP, De Baere E. CEP290, a gene with many faces: mutation overview
684 and presentation of CEP290base. *Hum Mutat*. 2010;31(10):1097-108. doi: 10.1002/humu.21337. PubMed PMID:
685 20690115.

686 62. Perrault I, Delphin N, Hanein S, Gerber S, Dufier JL, Roche O, et al. Spectrum of NPHP6/CEP290
687 mutations in Leber congenital amaurosis and delineation of the associated phenotype. *Hum Mutat*. 2007;28(4):416.
688 Epub 2007/03/09. doi: 10.1002/humu.9485. PubMed PMID: 17345604.

689 63. Feldhaus B, Weisschuh N, Nasser F, den Hollander AI, Cremers FPM, Zrenner E, et al. CEP290 Mutation
690 Spectrum and Delineation of the Associated Phenotype in a Large German Cohort: A Monocentric Study.

691 American journal of ophthalmology. 2020;211:142-50. Epub 2019/11/18. doi: 10.1016/j.ajo.2019.11.012.
692 PubMed PMID: 31734136.

693 64. Paloma E, Martinez-Mir A, Vilageliu L, Gonzalez-Duarte R, Balcells S. Spectrum of ABCA4 (ABCR)
694 gene mutations in Spanish patients with autosomal recessive macular dystrophies. Hum Mutat. 2001;17(6):504-
695 10. Epub 2001/06/01. doi: 10.1002/humu.1133. PubMed PMID: 11385708.

696 65. Apfelstedt-Sylla E, Theischen M, Ruther K, Wedemann H, Gal A, Zrenner E. Extensive intrafamilial and
697 interfamilial phenotypic variation among patients with autosomal dominant retinal dystrophy and mutations in the
698 human RDS/peripherin gene. Br J Ophthalmol. 1995;79(1):28-34. Epub 1995/01/01. doi: 10.1136/bjo.79.1.28.
699 PubMed PMID: 7880786; PubMed Central PMCID: PMCPMC505014.

700 66. Boon CJ, den Hollander AI, Hoyng CB, Cremers FP, Klevering BJ, Keunen JE. The spectrum of retinal
701 dystrophies caused by mutations in the peripherin/RDS gene. Progress in retinal and eye research. 2008;27(2):213-
702 35. Epub 2008/03/11. doi: 10.1016/j.preteyeres.2008.01.002. PubMed PMID: 18328765.

703 67. Del Pozo-Valero M, Martin-Merida I, Jimenez-Rolando B, Arteche A, Avila-Fernandez A, Blanco-Kelly
704 F, et al. Expanded Phenotypic Spectrum of Retinopathies Associated with Autosomal Recessive and Dominant
705 Mutations in PROM1. American journal of ophthalmology. 2019;207:204-14. Epub 2019/05/28. doi:
706 10.1016/j.ajo.2019.05.014. PubMed PMID: 31129250.

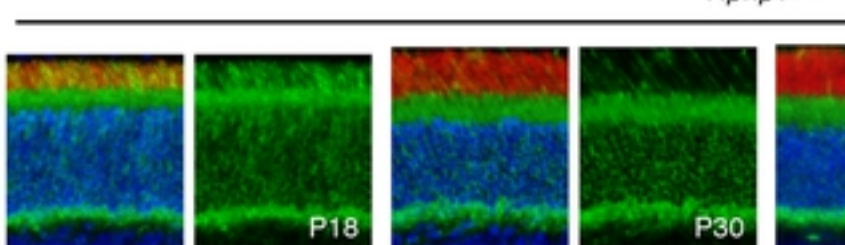
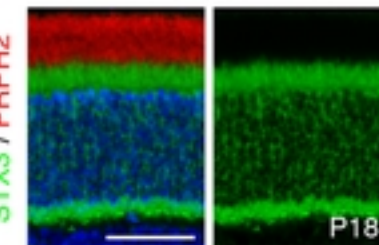
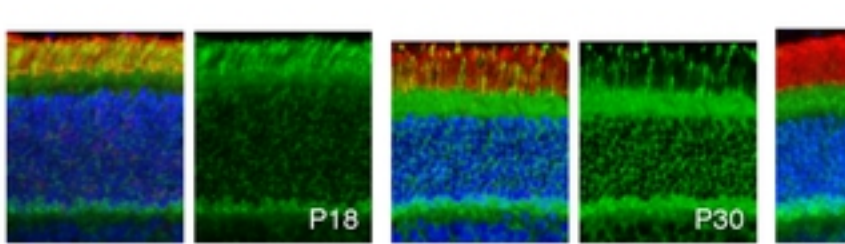
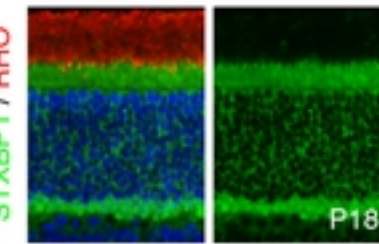
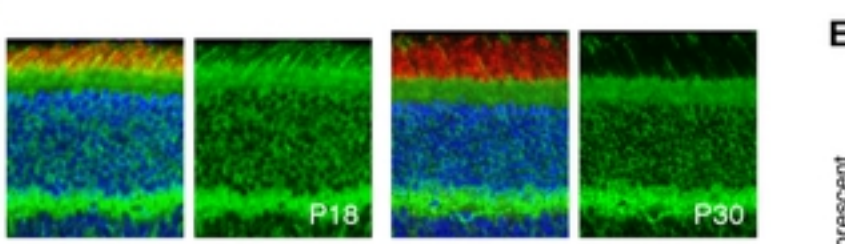
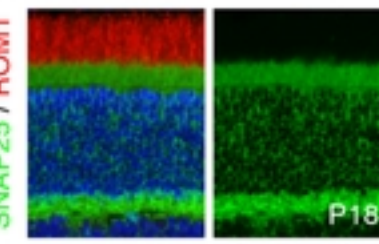
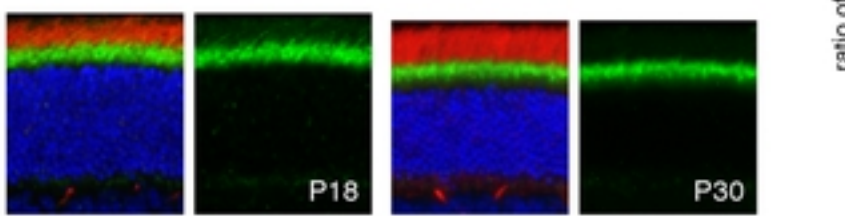
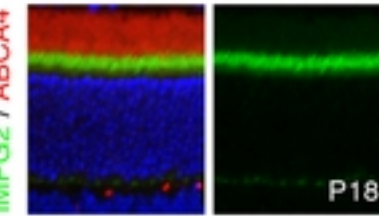
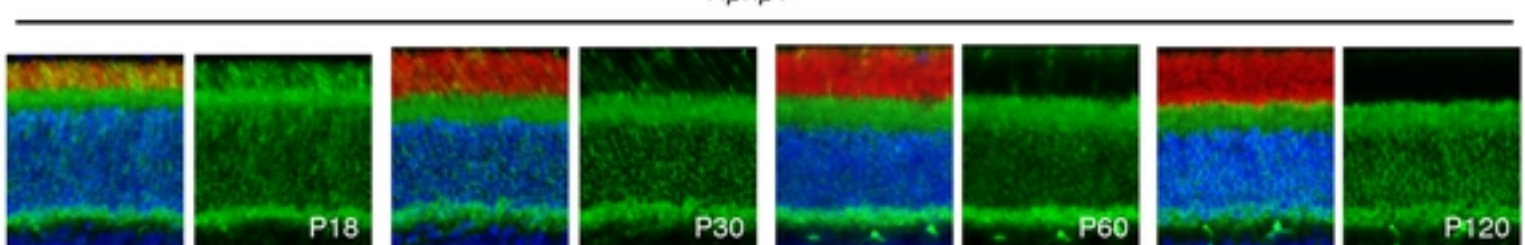
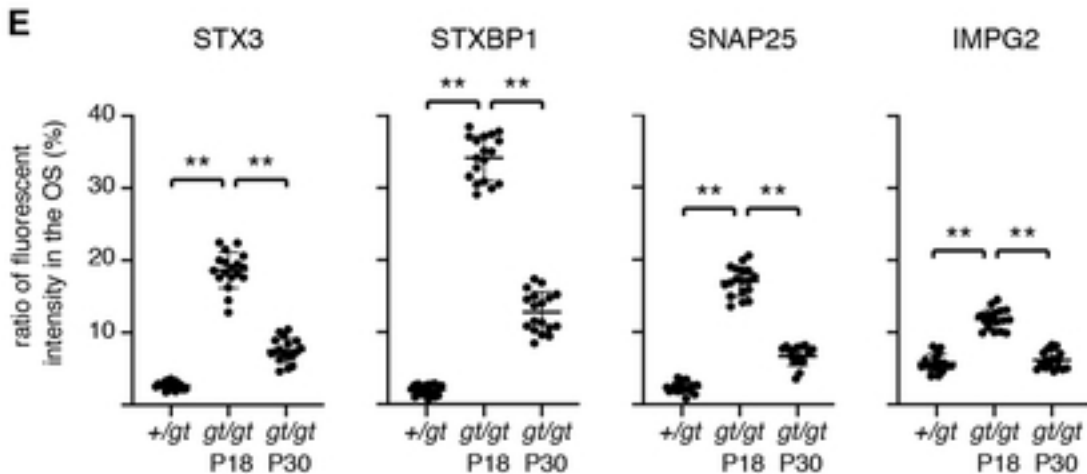
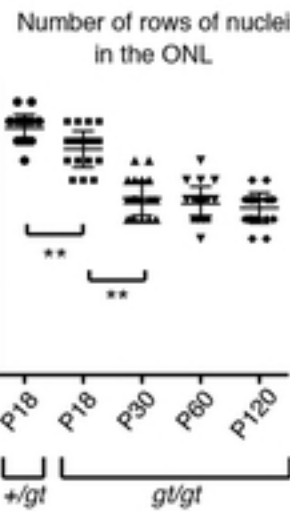
707 68. Mou H, Smith JL, Peng L, Yin H, Moore J, Zhang XO, et al. CRISPR/Cas9-mediated genome editing
708 induces exon skipping by alternative splicing or exon deletion. Genome Biol. 2017;18(1):108. Epub 2017/06/16.
709 doi: 10.1186/s13059-017-1237-8. PubMed PMID: 28615073; PubMed Central PMCID: PMCPMC5470253.

710 69. Lalonde S, Stone OA, Lessard S, Lavertu A, Desjardins J, Beaudoin M, et al. Frameshift indels introduced
711 by genome editing can lead to in-frame exon skipping. PLoS One. 2017;12(6):e0178700. Epub 2017/06/02. doi:
712 10.1371/journal.pone.0178700. PubMed PMID: 28570605; PubMed Central PMCID: PMCPMC5453576.

713 70. Anderson JL, Mulligan TS, Shen MC, Wang H, Scahill CM, Tan FJ, et al. mRNA processing in mutant
714 zebrafish lines generated by chemical and CRISPR-mediated mutagenesis produces unexpected transcripts that
715 escape nonsense-mediated decay. PLoS Genet. 2017;13(11):e1007105. Epub 2017/11/22. doi:
716 10.1371/journal.pgen.1007105. PubMed PMID: 29161261; PubMed Central PMCID: PMCPMC5716581.
717

718 Abbreviations

719 DAPI: 4',6-Diamidine-2'-phenylindole dihydrochloride
720 DMEM: Dulbecco's modified Eagle's medium
721 CRISPR: clustered regularly interspaced short palindromic repeats
722 ERG: electroretinogram
723 IS: inner segment
724 JBTS: Joubert syndrome
725 LCA: Leber congenital amaurosis
726 MKS: Meckel-Gruber syndrome
727 NPHP: nephronophthisis
728 ONL: outer nuclear layer
729 OPL: outer plexiform layer
730 OS: outer segment
731 RT-PCR: reverse transcription polymerase chain reaction
732 SD: standard deviation

A*Nphp1*^{+/gt}**B****C****D***Nphp1*^{gt/gt}**E****F****Fig 1**

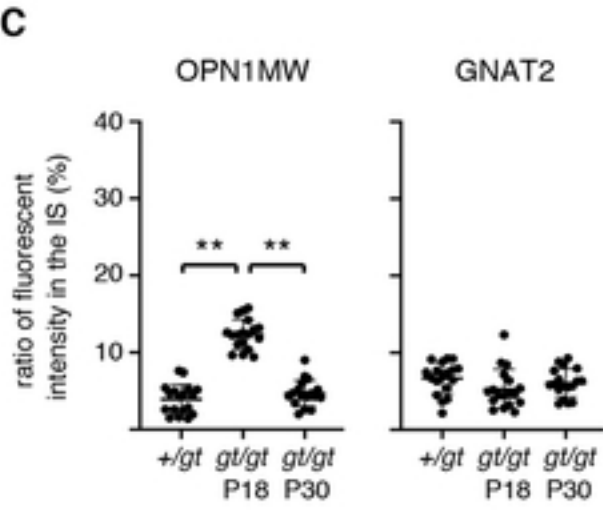
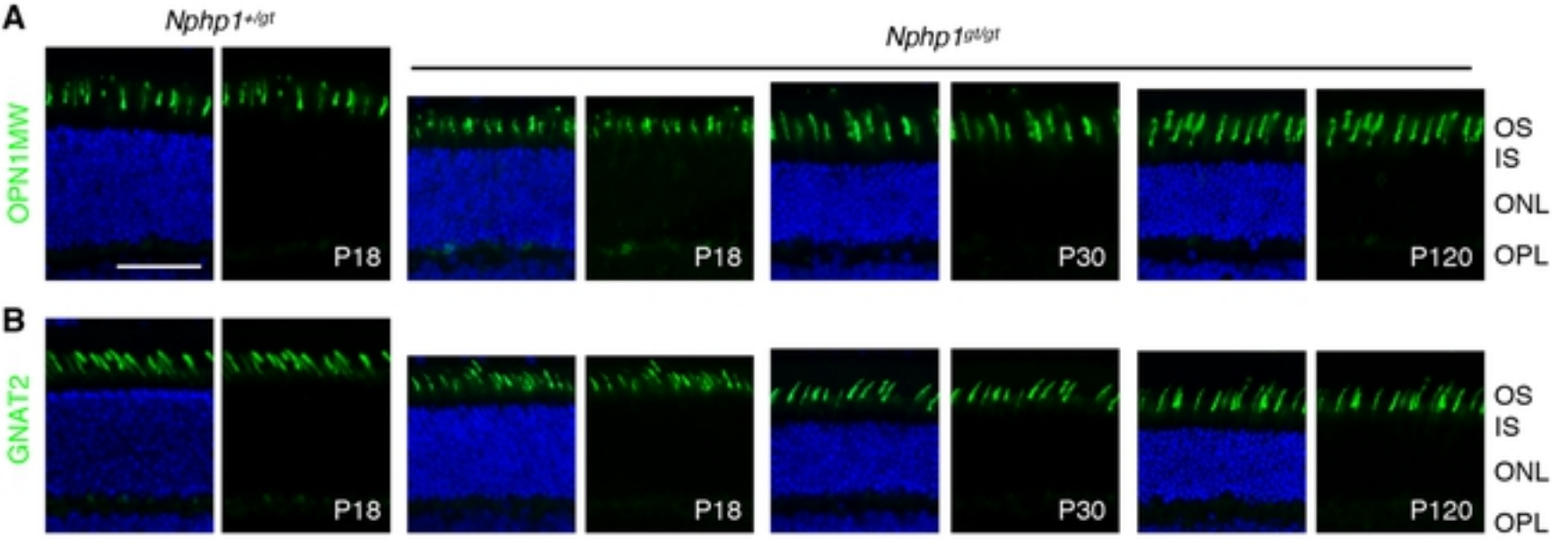


Fig 2

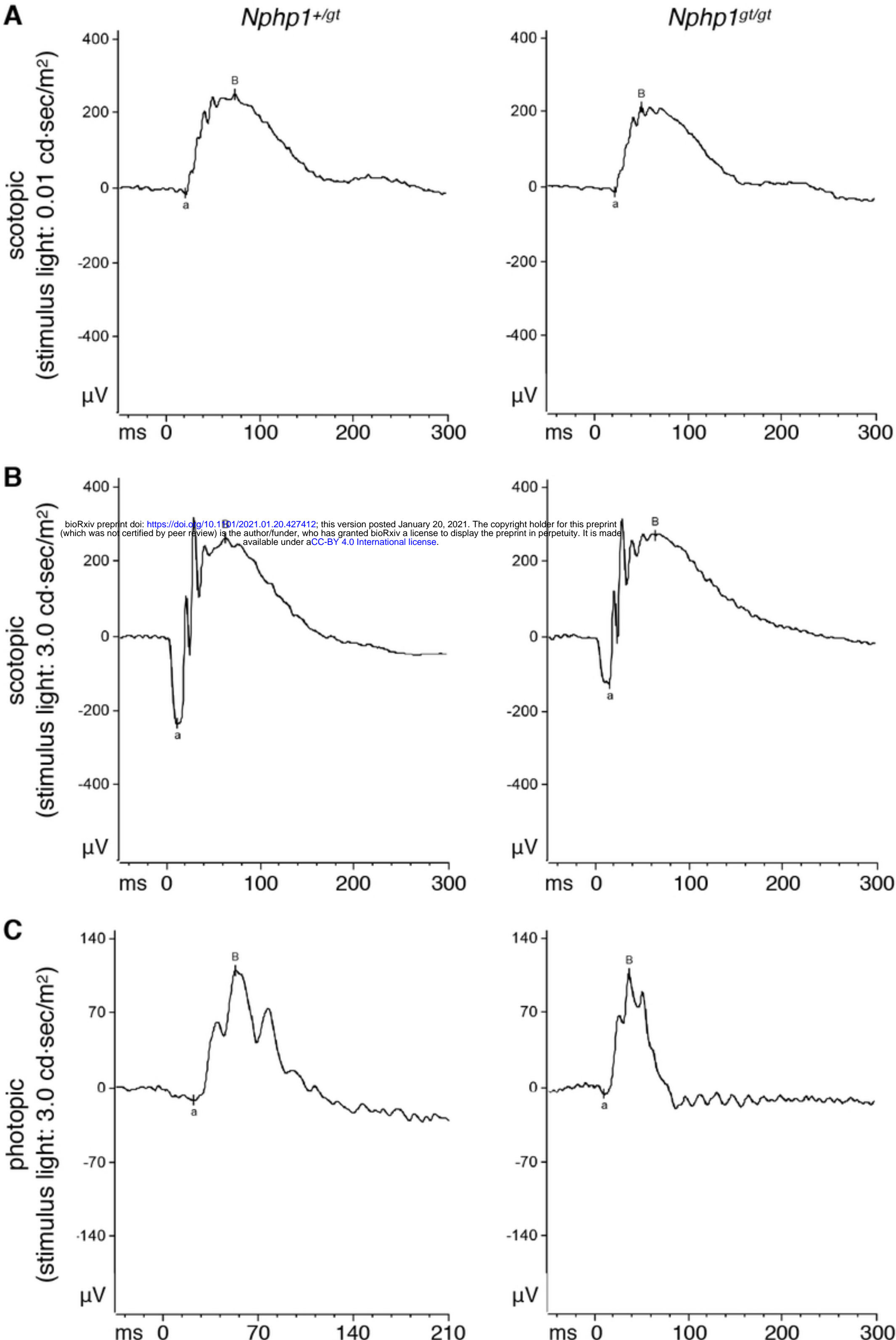


Fig 3

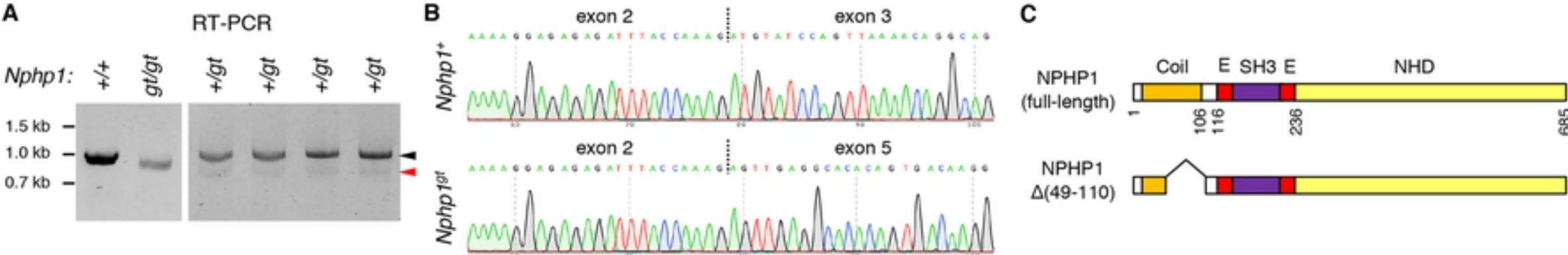


Fig 4

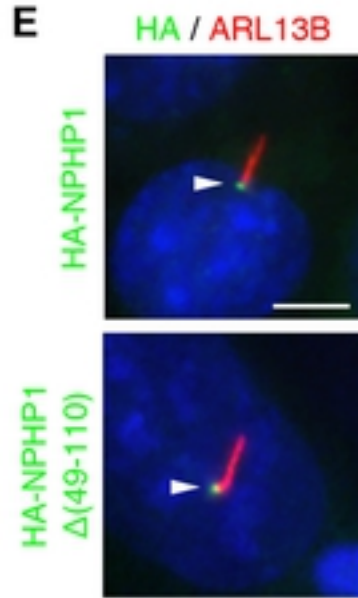
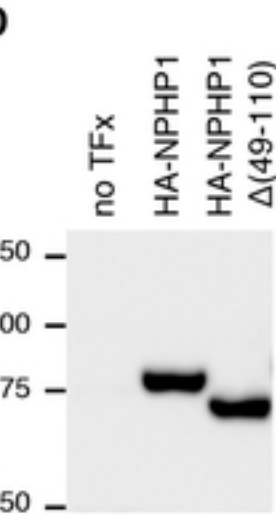
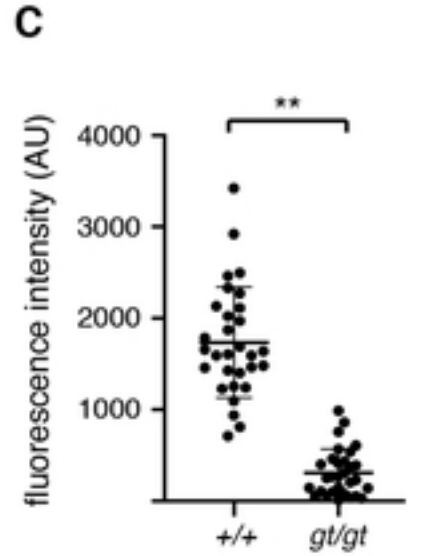
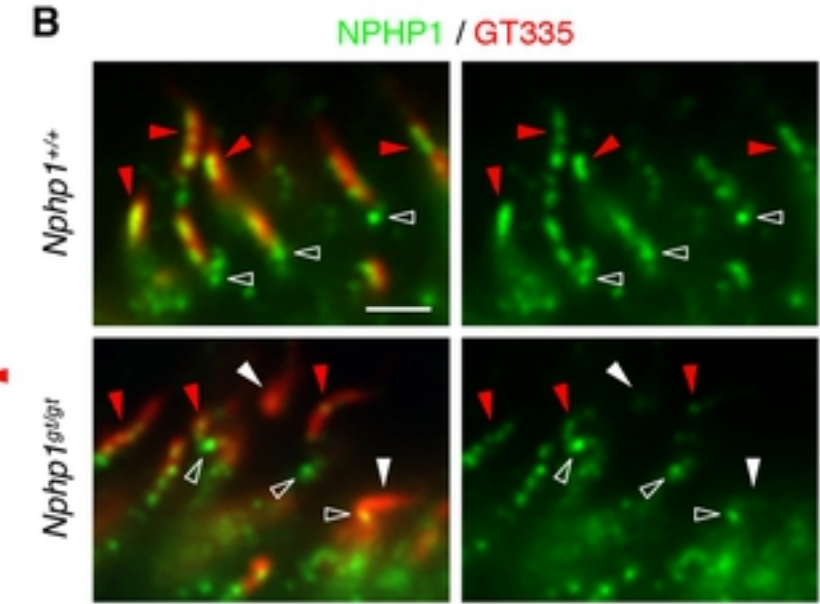
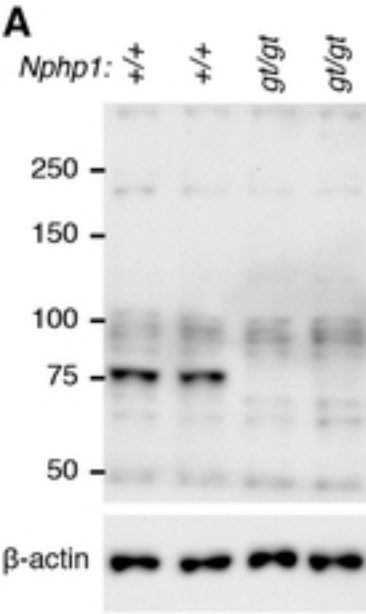


Fig 5

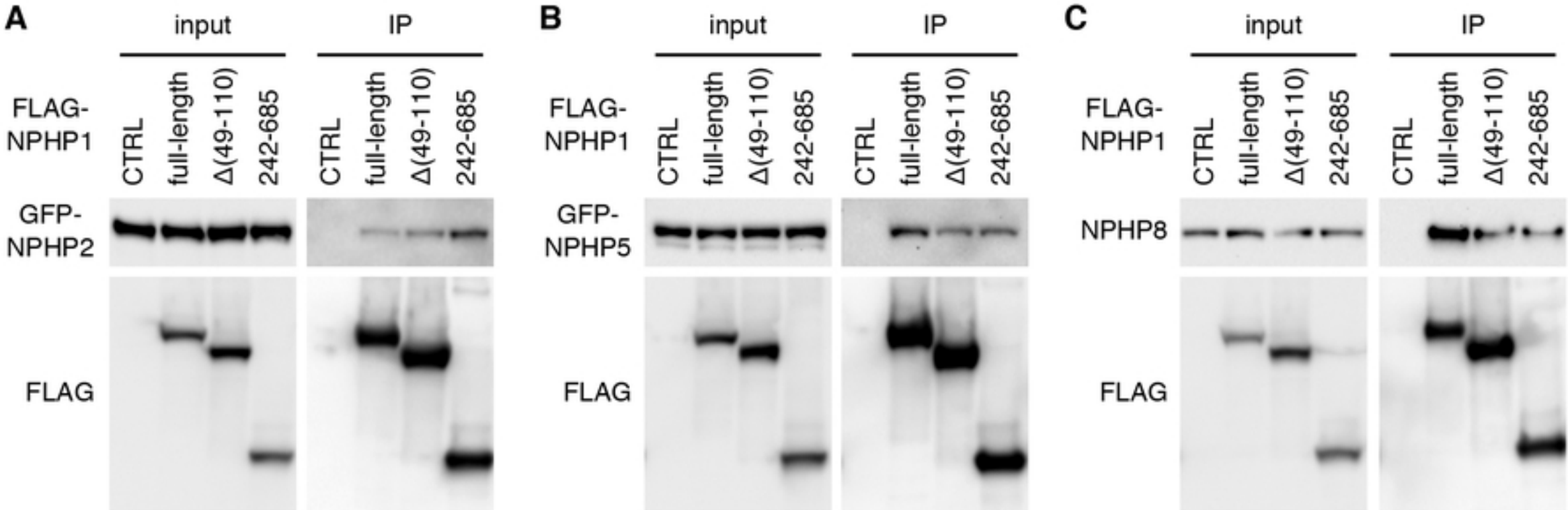
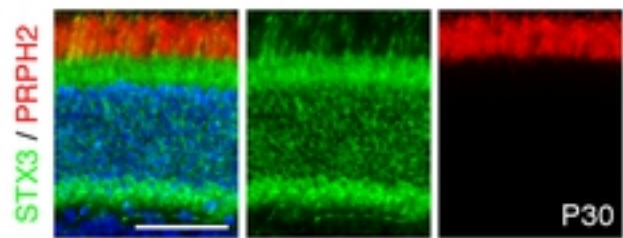
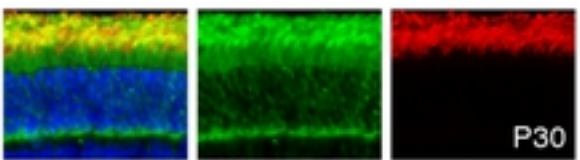


Fig 6

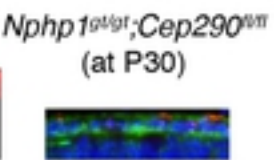
A *Nphp1^{gt/gt};Cep290^{+/+}*



Nphp1^{gt/gt};Cep290^{+/+}

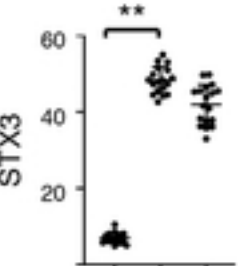


P30

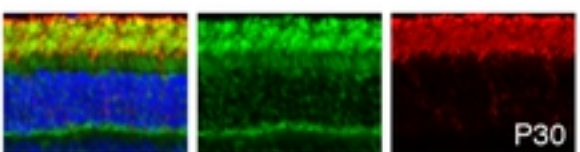
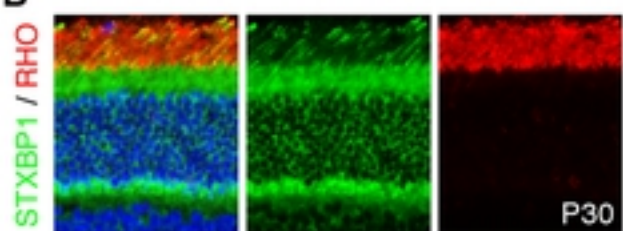


P60

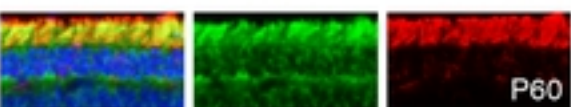
Ratio of fluorescent intensity in the OS (%)



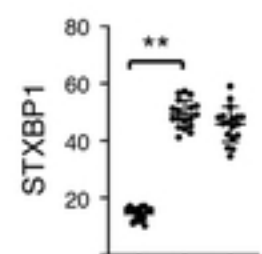
B



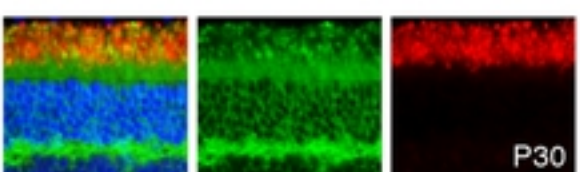
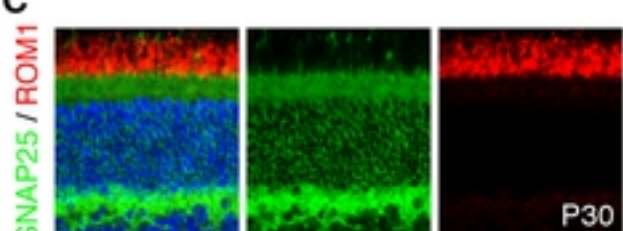
P30



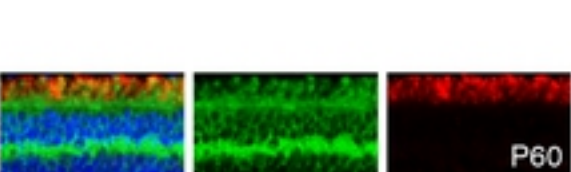
P60



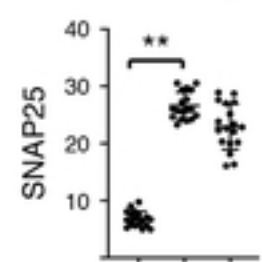
C



P30



P60



Cep290: $^{+/+}$; P30 $^{+/-}$; P30 $^{+/-}$; P60

Fig 7